

Oscillatory patterns in the light curves of 5 long-term monitored type 1 AGN

Andjelka B. Kovačević,^{1*} Ernesto Pérez-Hernández,² Luka Č. Popović,^{1,3}
 Alla I. Shapovalova,⁴ Wolfram Kollatschny⁵ and Dragana Ilić¹

¹*Department of Astronomy, Faculty of Mathematics, University of Belgrade, Studentski trg 16, Belgrade 11000, Serbia*

²*Departamento de Física, Universidad de Guadalajara, Revolución 1500, 44420 Guadalajara, Jalisco, México*

³*Astronomical Observatory, Volgina 7, Belgrade 11060, Serbia*

⁴*Special Astrophysical Observatory of the Russian Academy of Science, Nizhnij Arkhiz, Karachaevo-Cherkesia 369167, Russia*

⁵*Institut für Astrophysik, Universität Göttingen, Friedrich-Hund Platz 1, 37077 Göttingen, Germany*

Accepted XXX. Received YYY; in original form ZZZ

ABSTRACT

A new combined data of 5 well known type 1 AGN are probed with a novel hybrid method in a search for oscillatory behavior. Additional analysis of artificial light curves obtained from the coupled oscillatory models gives confirmation for detected periods that could have physical background. We find periodic variations in the long-term light curves of 3C 390.3, NGC 4151, NGC 5548 and E1821+643, with correlation coefficients larger than 0.6. We show that oscillatory patterns of two binary black hole candidates NGC 5548 and E1821+643 corresponds to qualitatively different dynamical regimes of chaos and stability, respectively. We demonstrate that absence of oscillatory patterns in Arp 102B could be due to a weak coupling between oscillatory mechanisms. This is the first good evidence that 3C 390.3 and Arp 102B, categorized as double-peaked Balmer line objects, have qualitative different dynamics. Our analysis shows a novelty in the oscillatory dynamical patterns of the light curves of these type 1 AGN.

Key words: galaxies:active – galaxies:nuclei –galaxies: Seyfert – galaxies supermassive black holes – methods: data analysis

1 INTRODUCTION

The optical emission of Active Galactic Nuclei (AGN) is of great complexity, containing the stellar component, the emission lines from narrow line region and broad line region (BLR), the black body emission of the accretion disc which is orbiting a supermassive black hole (SMBH), the re-emission from the molecular torus obscuring the accretion disc, and synchrotron and inverse Compton emissions (see e. g. Netzer 2013, and references therein). Hence, optical variability studies give insight in geometry, physics and dynamics of AGN (Rees 1984; Torricelli-Campioni et al. 2000; Hawkins 2002; Sesar et al. 2007; Mushotzky et al. 2011), but the used data must cover long time periods (Webb et al. 1988). Because of this, AGN long-term monitoring programs are crucial for understanding physical aspects of AGN as well as for establishing cosmological constrains due to the wide distribution of AGN over different cosmological time-scales (Hönig 2014; Risaliti & Lusso 2017). Long-term light curves are valuable to deal with open questions concerning AGN, particularly about possible periodicities and their physical origin (see Li et al. 2016; Lu et al. 2016, and ref-

erences therein). Searching for periodicity has been an important topic of AGN variability studies for about 4 decades, because confirmed periodicity would strongly limit the possible physical models and would help us determine the relevant physical parameters in AGN (Lainela et al. 1999). Additionally, oscillatory patterns immersed in AGN light curves represent higher level structures in the time series, which are suitable for comparative analysis of these objects.

The time series investigation methods can be classified as shape-based, structure-based (or model-based), and dimensionality reduction (Ding et al. 2008). The dimensionality reduction methods are based on data transformation such as discrete Fourier transformation, single value decomposition, continuous wavelet transformation (CWT) and discrete wavelet transformation (DWT), piecewise approximation, and Chebyshev polynomials.

Mostly, time-series analysis of AGN attempts to characterize the similarity between curves based on their shape (i. e. utilizing Euclidean characteristics). For long time series, as are AGN long-term monitored data, structure-based and dimensionality reduction methods could be more effective (Tenenbaum et al. 2000; Keogh et al. 2001; Wang & Megalooikonomou 2008; Aghabozorgi et al. 2015). Shape-based methods, being based on Euclidean metric,

* E-mail: andjelka@matf.bg.ac.rs

compare only time series of the same length, does not handle outliers or noise, and they are very sensitive to signal transformations, phase shifts of signals, time delays, unsynchronized signals, etc. On the other hand, structure-based approaches look for latent similarities, usually by transforming series into a new domain, where similarity can be more evident. These methods can extract global features from the time series, and creating vectors of them can be also used to measure similarity and/or classify objects.

A higher level information hidden in AGN light curves- oscillatory patterns have been proposed to underlie variability phenomena in numerous AGN with the extent of periods from a few days to a few decades (see [Charisi et al. 2016](#), and references therein). In other words, even if red noise is present in AGN light curves, there is a non-negligible probability of detecting periodic behavior ([Leighly 2005](#)). On the other hand, different values for the periods can also be derived, which depends on the data set and adopted method for testing ([Kudryavtseva & Pyatunina 2006](#)). Thus it might be important to examine whether the results remain robust when the periodicity problem is investigated by a somewhat different method with limitations that light curves are combined from different monitoring campaigns.

Based on the above discussion, the aim of present paper is twofold. Firstly, to utilize a new data sets of 5 well known type 1 AGN, combined from several well documented long term monitoring campaigns, and then to detect periodicity in the combined light curves using a novel method. Secondly, to construct models capable to reproduce oscillatory patterns and phase space dynamics of the combined light curves, and to find physical relevance of detected oscillatory patterns.

The paper is organized as follows. In section 2 we describe the used AGN sample, their time series and method for detection of oscillatory patterns and phase trajectory calculation. Section 3 focuses in detail on the results of the application of proposed hybrid method for periodicity detection. Section 4 gives a new comparative analysis of oscillatory patterns and phase-space dynamics of combined and modeled light curves and Section 5 summarizes the main conclusions.

2 DATA AND PERIODICITY ANALYSIS

In the following, we briefly describe data sets of selected AGN, and then discuss methods and models used for the periodicity analysis. In particular we present for the first time the combined light curves: the continuum 6200 Å, and H α of Arp 102B, the continuum 5100 Å, H α and H β of 3C 390.3 and the continuum 5100 Å, and H β of NGC 4151. The combined light curves of NGC 5548 have been already published as well as the light curves of E1821+643, so their plots will not be repeated here (see references listed in Table 1 for details).

2.1 The light curves

An ideal data of ideal periodic phenomena would perhaps satisfy conditions of Nyquist theorem, so that a light curve with the duration of about 1.5 – 2 times longer than the claimed periodicity would be enough for period measurement. However, due to the transient nature of underlying oscillatory patterns caused by unfavorable characteristics of observed light curves (e.g. signal to noise ratio, systematic errors, irregularities), long term light curves are needed to establish a key aspect of periodic patterns in case of observed data ([Fan et al. 1997](#)). Existing optical light curves from

different monitoring campaigns have been analyzed by different methods, but the information that can be derived from these observations has not been depleted. One of the possibilities is to combine these data into composite light curves, which could benefit longer time baselines and better sampling.

The characteristics of these objects encompasses the entire range of type 1 AGN activity (see Table 1): from Seyfert 1 objects NGC 4151 and NGC 5548 as prototypes of spectral type variation (from Seyfert 1.0 to 1.8), a very broad line and radio loud object 3C 390.3, then Arp 102B that is considered as a LINER and archetypical disc accretion emitter due to extremely broad, double peaked Balmer lines, and finally radio quiet but optically powerful nearby quasar E1821+643. Table 1 lists general information for each object: object name, AGN type, redshift, total period of monitoring programs, the combined light curve used for the analysis, mean sampling of the combined light curves, as well as the variability parameter- excess variance (see eq. (7) in [Simm et al. 2015](#), and references therein), and finally references from which the observations were taken.

We note that the AGN Black Hole Mass Database (AGNBHMD [Bentz & Katz 2015](#)) refers to a large number of published spectroscopic reverberation-mapping studies of AGN. But for our purpose we combined datasets for each object as follows:

- (i) For NGC 5548, we used the light curves given in [Bon et al. \(2016\)](#). The continuum 5100 Å and H β line are covering remarkable four decades long time span (see their Fig. 2);
- (ii) For Arp 102B (see Fig. 1), we combined datasets of [Shapovalova et al. \(2013\)](#), spanning the period of 1987-2010) and [Sergeev et al. \(2000\)](#), covering the period of 1992-1996);
- (iii) For 3C 390.3, Fig. 2, the used observations are from [Dietrich et al. \(1998\)](#), covering period 1994-1995), [Dietrich et al. \(2012\)](#), covering period from September till December 2005), [Shapovalova et al. \(2010a\)](#), covering period 1995-2007), [Sergeev et al. \(2011\)](#), covering period 2000-2007) and [Afanasyev et al. \(2015\)](#), covering period 2009-2014). Due to complexity of this object, it might be useful to search for periodicity information hidden in the other wavebands, i. e. the continuum 1370 Å, Ly α and CIV lines collected by IUE satellite from 1978-1992 ([Wamsteker et al. 1997](#)) and from 1994 December to 1996 March ([O' Brien et al. 1998](#));
- (iv) For NGC 4151, Fig. 3, the light curves include observations from [Kaspi et al. \(1996\)](#), covering period over two months in 1993), from [Shapovalova et al. \(2010b\)](#), covering period 1996-2006), and finally we added two observations presented in [Bon et al. \(2012\)](#), one from 1986, and other from 1989);
- (v) Up to now, for E1821+643 the only information available are fluxes obtained from its the first long term (1990-2014) monitoring campaign conducted by [Shapovalova et al. \(2016\)](#), see their Fig. 5.

2.2 Methods

Almost all AGN light curves show neither apparent periodicity nor typical time-scale. Their variations look like each other from largest (years) up to the smallest time-scales (hours). Namely, AGN fluxes exhibit self-similar or fractal variations ([Kawaguchi & Mineshigei 1999](#)). On the contrary, detection of a periodic variation in AGN light curves which would resemble the supermassive binary black hole orbital time-scales are highly desirable ([Popović 2012](#)). Such signals are weak, with long time-scale (i. e. low frequency [Netzer 2013](#)) and immersed in the fractal and noisy structure of AGN time series. Usually, low-frequency filtering methods require a certain prior knowledge of the expected range of periodic signal (such as

Table 1. AGN sample for testing periodic variability. Columns are: object name, AGN type, redshift, total period of monitoring programs, the combined light curve, mean sampling of the combined light curve, excess variance of the combined light curves, literature from which combined light curves were compiled.

Object name	Type	z	Period	CLC	Sampling (days)	EV	Reference ^a	
3C 390.3	BLRG	0.056	1994-2014	Continuum 5100 Å	11.6	0.1623	1, 2, 3, 4, 5	
				H α	34.5	0.1055		
			H β	20.5	0.1099			
			1978-1996	Continuum 1370 Å	64.4	0.1737		6, 7
				Ly α	64.4	0.2539		
Arp 102b	LINER	0.024	1987-2010	Continuum 6200 Å	78.1	0.0080	8, 9	
				H α	77.0	0.0245		
				Continuum 5100 Å	73.0	0.0073		
				H β	60.0	0.0090		
NGC 4151	Seyfert 1	0.003	1993-2006	Continuum 5100 Å	16.1	0.2847	10,11, 12	
			1986-2006	H α	39.6	0.0740		
			1993-2006	H β	19.2	0.1367		
NGC 5548	Seyfert 1	0.017	1972-2015	Continuum 5100 Å	6.9	0.0648	13	
				H β	11.2	0.0917		
E1821+643	Quasar	0.297	1990-2014	Continuum 5100 Å	68.4	0.0357	14	
				H β	68.4	0.0049		
				Continuum 4200 Å	114.9	0.0359		
				H γ	114.9	0.0356		

^a (1) Dietrich et al. (1998), (2) Shapovalova et al. (2010a), (3) Dietrich et al. (2012), (4) Sergeev et al. (2011), (5) Afanasiev et al. (2015), (6) Wamsteker et al. (1997), (7) O’ Brien et al. (1998), (8) Shapovalova et al. (2013), (9) Sergeev et al. (2000), (10) Kaspi et al. (1996), (11) Shapovalova et al. (2010b), (12) Bon et al. (2012), (13) Bon et al. (2016), (14) Shapovalova et al. (2016).

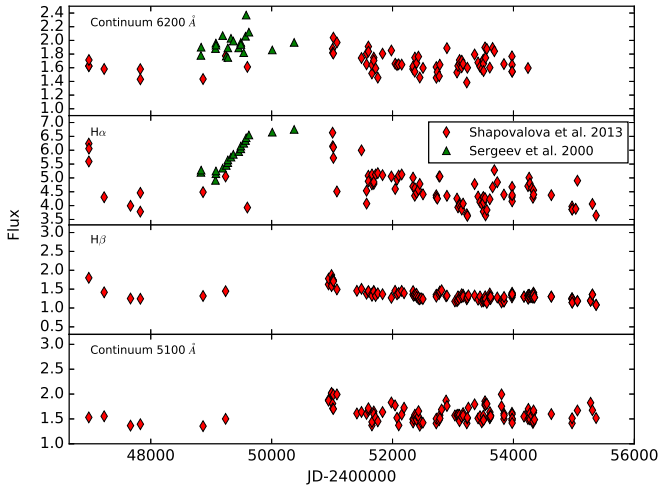


Figure 1. Combined light curves of Arp 102B covering the period of 1987 - 2010. From top to bottom: continuum flux at 6200 Å (94 points), H α and H β line fluxes (110 and 141 points respectively), and continuum flux at 5100 Å (116 points). The continuum fluxes are in units of $10^{-15} \text{ ergs s}^{-1} \text{ cm}^{-2} \text{ \AA}^{-1}$, and the line fluxes are in units of $10^{-13} \text{ ergs s}^{-1} \text{ cm}^{-2}$. Observations from different campaigns are marked by different colors given in legend on the second subplot from the top.

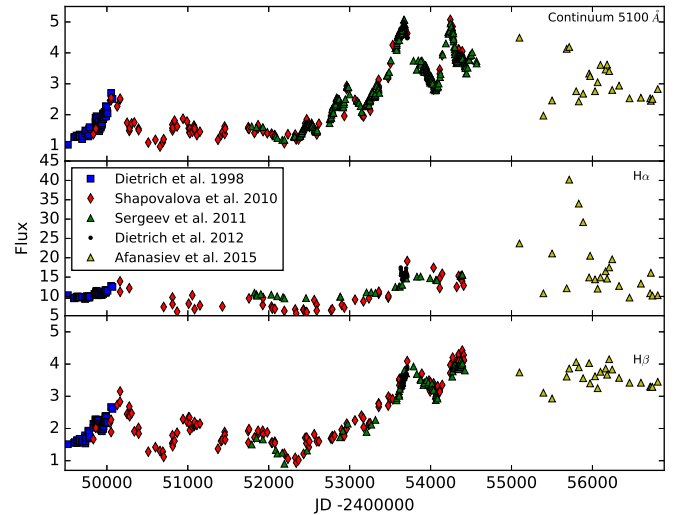


Figure 2. Combined light curves of 3C 390.3 covering the period of 1995 - 2014. From top to bottom: continuum flux at 5100 Å (630 points), H α and H β line fluxes (212 and 356 points, respectively). The continuum flux is in units of $10^{-15} \text{ ergs s}^{-1} \text{ cm}^{-2} \text{ \AA}^{-1}$, and the line fluxes are in units of $10^{-13} \text{ ergs s}^{-1} \text{ cm}^{-2}$. Observations from different campaigns are marked by different colors given in legend on the second subplot from the top.

frequency, phase, etc.). However, problems we are encountering are detection of a periodic signal in light curves when we do not know *a priori* that such signal exists or about its characteristics.

To address such situation, we proposed a hybrid method to detect unknown weak periodic signals in the AGN light curves, which is a modification of the recently proposed timing methods used

in geophysics (Pering et al. 2014) and acoustics research (Yang & Tse 2005). Pering et al. (2014) method identifies the fundamental frequencies of transient oscillations in two time series by means of Spearman’s rank correlation coefficient analysis of CWT of used data. Their approach is a fusion of the CWT analysis (suited

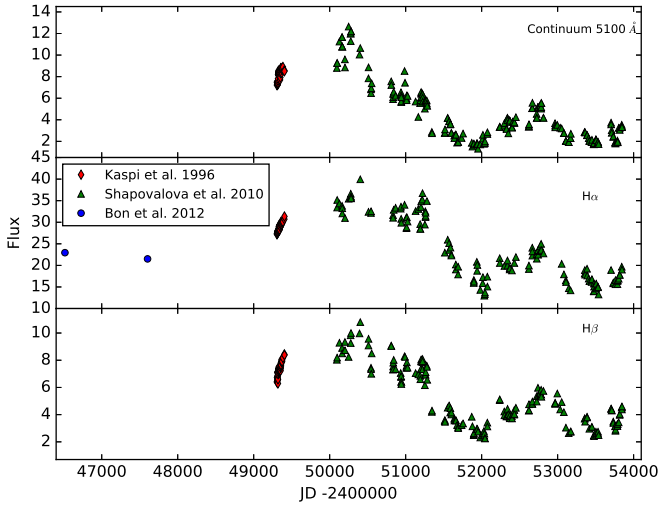


Figure 3. Combined light curves of NGC 4151 covering the period of 1993 - 2010. From top to bottom: continuum flux at 5100 Å (283 points), H α and H β line fluxes (168 and 238 points, respectively). The continuum flux is in units of 10^{-14} ergs s^{-1} cm^{-2} \AA^{-1} , and the line fluxes are in units of 10^{-12} ergs s^{-1} cm^{-2} . Observations from different campaigns are marked by different colors given in legend on the second subplot from the top.

for investigation of transient or unstable periodic phenomena), and Spearman correlation technique that accounts for non-linearity and variable amplitude of the wavelet coefficients.

To account for the irregular sampling in our data sets, we use Gaussian process regression (GP), an approach that has been applied successfully in recent stochastic simulation/interpolation studies which quantified variability of quasar light curves with arbitrary sampling (see Pancoast et al. 2015a,b; Grier et al. 2017, and references therein). Beside the interpolation between data points, GP also makes self consistent estimates and allows us to incorporate the measurement errors while making minimal assumptions about the exact form of activity of the object. It allows for a more flexible model which capitalizes on the data available and can model subtle but important differences within the data. To compensate the heavy influence of the recent data which are better sampled, we interpolated AGN light curves by means of GP obtaining 1-day sampled light curves. This time interval is short enough in comparison to the long-term periods (years) and thus can barely perturb the long-term variations. The GP approach is based upon choice of a kernel. For the calculations shown here, we utilized Ornstein-Uhlenbeck (OU) kernel, since sometimes it is a good descriptor of quasar variability (see Zheng et al. 2016, and references therein). As a caution, we should note that OU (or damped random walk) may not be ideal for Seyferts or for all frequencies. For example Mushotzky et al. (2011) showed that the steep power spectra are inconsistent with the damped random walk, which is also confirmed in the analyses by Kozłowski. (2017) and Guo et al. (2017). For details about OU covariance function (kernel) see Kovačević et al. (2017, and references therein). Moreover, as the light curves seem to be sparsely sampled over long monitoring time, we show the examples of comparison between the GP interpolated and observed light curves in Fig. 4. To exhibit parallels between fitted models, the observed curves were normalized to maximal flux.

Instead of calculation of CWT coefficients of the time series, our method determines bandpass envelope of given curves based

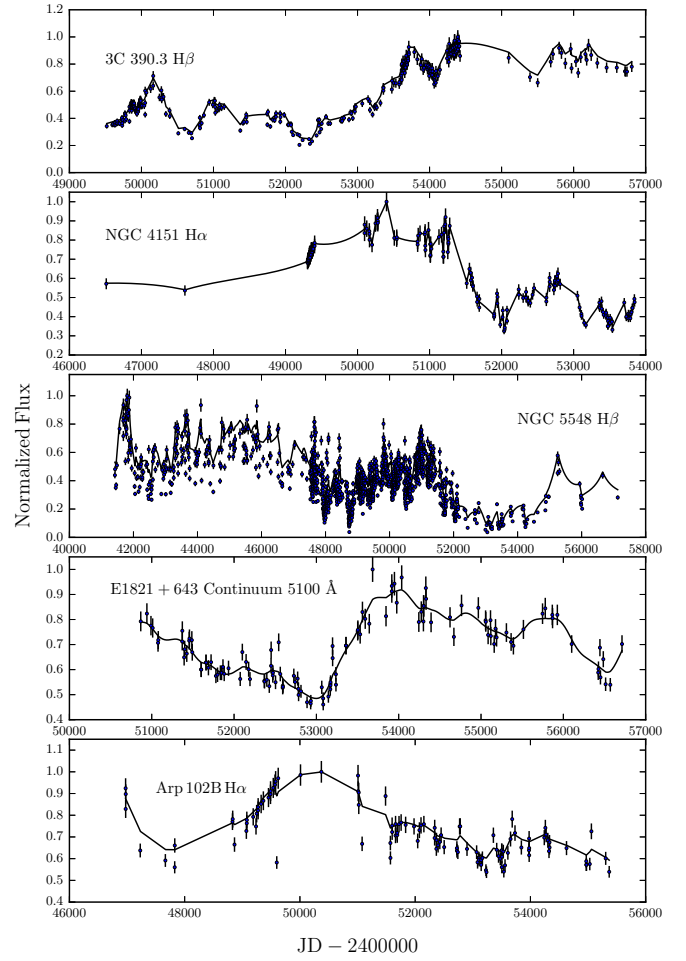


Figure 4. Examples of the comparison between the GP posterior mean (solid line) and observed light curves (dots) for the five objects. Names of the objects and light curves are given in each subplot.

on the complex Morlet wavelet function. Yang & Tse (2005) have shown in acoustic analysis that this approach substantially mitigates overlapping and noise-induced signal. We choose the complex mother wavelet function because it possesses two degrees of freedom (its real and imaginary part) to probe for structure in the time series. The complex Morlet wavelet transform of time series $x(t)$ at an arbitrary scale a and for translational parameter b can be formulated as (Yang & Tse 2005)

$$\text{CWT}(a, b) = \frac{1}{\sqrt{2\pi a}} \int_{-\infty}^{+\infty} x(t) e^{[(t/b)^2/a/2]\beta^2} e^{i\omega(t-b)/a} dt \quad (1)$$

where $i = \sqrt{-1}$, ω is frequency of the wavelet function and β is parameter controlling the wavelet function's shape. Physically, $\text{CWT}(a, b)$ is the energy of $x(t)$ in scale a at time $t = b$. Then the envelope ($\text{env}(a, b)$) of the wavelet coefficients are given by the following metric expression (Yang & Tse 2005)

$$\text{env}(a, b) = \sqrt{\text{Re}[(\text{CWT}(a, b))^2] + \text{Im}[(\text{CWT}(a, b))^2]} \quad (2)$$

where Re, Im stand for the real and the imaginary part of a given CWT.

The next step is to calculate correlation coefficients of the envelopes of the wavelet coefficients of each light curve at each wavelet scale using Spearman rank correlation coefficient. Spearman's coefficient measure statistical dependence between two variables without a normality assumption for the underlying population (i.e. it is nonparametric measure). Since it uses the ranks of the values in two variables, instead of their numerical values, it is suitable for finding correlations in non-linear data and it is less sensitive to outliers. A confidence interval for correlation coefficient is constructed using Fisher's z transformation (see [Hollander et al. 1999](#); [Conover et al. 1999](#); [Altman et al. 2000](#)). The probability p associated with Spearman correlation coefficient is evaluated using an Edgeworth series approximation (see [Best & Roberts 1975](#)).

The level of match between oscillations presented in the two different light curves over a broad scale range can be visualized either as 3D correlation map (two axis are associated with periods in series and third is corresponding correlation coefficients) or in the form of 2D correlation map (two axes are corresponds to periods in two series while correlation coefficients are coded with different colors). Since the values of the position parameter b can be continuously varied, and the scaling a can be defined from the minimum (original signal scale) to a maximum chosen by the user, the CWT can be seen as a function of scales a as it is shown in [Grinsted et al. \(2004\)](#). For the Morlet wavelet the period is almost equal to the scale (see [Grinsted et al. 2004](#)). So the x and y axes of the correlation plots depicts scales a , or equivalently, periods. If the same period is presented in both light curves it will reveal itself in the high correlation regions centered on the 2D map's diagonal. The correlation between different periodicities (inter-oscillator correlation) would appear as regions of high correlation off the diagonal. The significance threshold for correlation coefficients was set at 0.005. We estimated periods by detecting peaks of correlation function which have largest correlation coefficients and p value below the significance threshold. The error of the resulting period (ΔP) was estimated formally as the half-width of the corresponding peak ([Kudryavtseva et al. 2011](#)).

2.3 Models

One of our ultimate goals is to give a physical interpretation to the obtained results. To do so, we constructed models that are capable to produce oscillatory and dynamical patterns similar to those found in our objects.

There are two types of such models: detailed and abstract (see [Nakao 2015](#), and references therein). Detailed models intend to exactly reproduce as many characteristics of the observed system as possible. Such models provide the quantitative understanding of the dynamical behavior of the studied system. The other class, abstract models can capture some essential aspect of the system, such as rhythmic behavior. Their purpose is not to faithfully simulate all aspects of dynamical behavior of observed system, but rather to describe some universal aspect of its dynamics. Since it is not focused on detailed behavior of any specific system, but rather on the universal characteristic of this behavior, it can give a unified frame for describing the behavior exhibited by a broad range of dynamical systems. Hence, such models allow us to accumulate a deeper comprehension of the general processes existing in broad classes of systems. For our purposes, the abstract models are suitable, simulating the network of coupled oscillatory processes ([Pikovsky, Rosenblum & Kurths 2001](#)). In such a model, the evolution of each oscillatory system is described by three degree of freedom, the amplitude, period (frequency), and the phase.

So, to investigate whether interactions between oscillators could contribute to the variety of oscillation patterns seen in AGN sample, we created two models.

The first type consists of two interacting units U_a, U_b , assuming that the interaction is linear and represented by the sum of one central and one remote oscillatory component. The guiding equations are given as follows

$$\begin{aligned} U_a(t) &= A(t) \cdot \sin(2\pi f_a t + \phi) + cp_{b \rightarrow a} \cdot \\ &B(t) \cdot \sin(2\pi f_b t + 2\pi f_b \tau) + W(t) \\ U_b(t) &= B(t) \cdot \sin(2\pi f_b t) + cp_{a \rightarrow b} \cdot \\ &A(t) \cdot \sin(2\pi f_a t + 2\pi f_a \tau + \phi) + W(t) \end{aligned} \quad (3)$$

where $A(t)$ and $B(t)$ are amplitudes of the central and remote oscillatory process before coupling occurs; $U_a(t), U_b(t)$ are outputs of two units at given time instance; f_a, f_b denote the frequencies of interest in U_a, U_b ; ϕ is the phase difference; τ is the delay between two units; $cp_{i \rightarrow j}$ is the connection strength between U_i to U_j , $i, j \in \{a, b\}$; and $W(t)$ is the red noise (i. e. Wiener process or Brownian motion). We generated $W(t)$ on the time interval $[0, T]$ as a random variable depending continuously on all $t \in [0, T]$ and satisfying conditions:

$W(0) = 0$, $W(t) - W(s) \sim \sqrt{(t-s)}N(0, 1)$ for $0 \leq s < t \leq T$. $N(0, 1)$ is the normal distribution with zero mean and unit variance, due to this fact, $W(t)$ is often called as Gaussian process. Note that for $0 \leq s < t < u < v \leq T$, $W(t) - W(s)$ and $W(v) - W(u)$ are independent. For use in our model, we discretize $W(t)$ with time step dt as $dW \sim \sqrt{dt}N(0, 1)$ and found its cumulative sum.

In difference to the first model, the second includes one central and two remote oscillatory component given as follows:

$$\begin{aligned} U_a(t) &= A(t) \cdot \sin(2\pi f_a t + \phi) + cp_{b \rightarrow a} \cdot \\ &B(t) \cdot \sin(2\pi f_b t + 2\pi f_b \tau) + cp_{c \rightarrow a} \cdot \\ &C(t) \cdot \sin(2\pi f_c t + 2\pi f_c \tau_1) + W(t) \\ U_c(t) &= B(t) \cdot \sin(2\pi f_b t) + C(t) \cdot \sin(2\pi f_c t) + cp_{a \rightarrow b} \cdot \\ &A(t) \cdot \sin(2\pi f_a t + 2\pi f_a \tau + \phi) + cp_{a \rightarrow c} \cdot \\ &A(t) \cdot \sin(2\pi f_a t + 2\pi f_a \tau_1 + \phi_1) + W(t) \end{aligned} \quad (4)$$

Additional remote oscillatory component has amplitude $C(t)$, frequency f_c , coupling strength to central oscillatory process (and vice versa) $cp_{a \rightarrow c}, cp_{c \rightarrow a}$, phase ϕ_1 and time delay τ_1 . The values for the variables in both models were set to the following: all parameters were always constant for considered time period, but were extracted from a normal Gaussian distribution for 100 reruns, separately for all involved oscillatory processes. In this way we have several degree of randomness: amplitudes, phases, red noise, and coupling parameter. Each trial of 2000 time points was defined in both models with resolution of 1 arbitrary chosen time unit.

To verify that similarities between real and modeled correlations maps are not accidental, we determined how dynamics of observed light curves compare to the dynamics defined by time-series models. To this intent, we calculated the phase trajectories of observed and modeled data, since phases are most sensitive to interaction, and provide description of connectivity within dynamical system which discloses a simple interpretation ([Kralemann et al. 2011](#)). The first step is to transform given time series $y(t) = (y_k(t)), k = 1, \dots, N$ of each object into a cyclic observable. This is completed via construction of a two-dimensional embed-

ding (y, y^H) (see [Kralemann et al. 2008](#), and references therein), where following equation

$$y^H(t) = \frac{1}{\pi} PV \int_{-\infty}^{\infty} \frac{y(\tau)}{t - \tau} d\tau \quad (5)$$

defines the Hilbert transform (HT) of time series $y(t)$ and PV indicates the Cauchy principal value ([Balanov et al. 2009](#)). To better understand the meaning of the HT, we can look at it from the point of view of a windowed sampling. The weight $\frac{1}{t-\tau}$ can be interpreted as a windowing width so the HT is a convolution integral of $y(t)$ with $\frac{1}{t}$. Therefore, equation (5) emphasizes the local properties of $y(t)$. To ensure existence of the integral, Lipschitz condition $|y(t_2) - y(t_1)| \leq L |t_2 - t_1|^\alpha$ must be satisfied by $y(t)$ on given time interval $[t_1, t_2]$, where L is a positive number. So if $\alpha = 0$ in an interval, $y(t)$ is discontinuous but bounded. We will not deal with Lipschitz condition here, however we will note that the most optical AGN time series satisfy it, since L can be found as a supremum of all differences in flux values.

The original signal ($y(t)$) and its HT ($y^H(t)$) then formulate a complex analytic signal in the following form

$$\tilde{y}(t) = y(t) + iy^H(t) \quad (6)$$

where $i = \sqrt{-1}$.

With this analytic signal, the time-dependent amplitude and phase information embedded in the original signal can be easily extracted. Since the HT amplitude is an index of vibratory energy and the phase is related to vibration frequency, such information is very desirable for characterizing dynamic characteristics of a system. HT is useful for long time series, low dimensional chaotic systems that exhibit transient chaos as well as for non stationary time series ([Lai & Ye 2003](#)). Alternatively, one can use for y^H the time derivative of y .

The similarity of underlying dynamics in observed and simulated light curves can be assessed by examining similarity of their phase trajectories in the phase space (y, y^H). If the oscillations are presented in the system, the phase trajectory in the plane (y, y^H) will be closed and can fill a certain annulus of phase space, called system's attractor ([Nekorkin 2015](#)). The absence of periodicity will be manifested in phase space through a non closed phase curve. If the underlying dynamics is random, then the trajectory has no definite shape and spreads all over the space. Moreover, if phase trajectories stay within a finite (i.e., bounded) range of distance away from the critical point they are stable. The phase space volume of system with conservative dynamics is preserved as time evolves, while phase space of dissipative dynamic system contracts as time evolves ([Grebogi et al. 1987](#)).

Finally, since determined periodicities are not obvious from visual inspection of observed light curves, it might be easier for the reader to discuss the reality of these variations on the basis of the comparison of the data and fitted sinusoids waveforms. Therefore, we applied multisinusoidal curves to perform the non-linear least square fitting of our data:

$$y = \sum_{i=1}^n c_i \sin\left(\frac{2\pi t}{p_i} + \phi_i\right) + B \quad (7)$$

where n stands for the number of detected periods in the light curves, y denotes observed fluxes, and t is corresponding time. From the fitting we estimate the following parameters: amplitudes c_i , periods p_i , phases ϕ_i and offset B which is a parameter that handles measurement data with non-zero mean value. As the archetypal periodic function, sinusoidal signal is a good reference point for

comparison to the observed light curves. The goodness of the fit is assessed by estimation of χ^2 and correlation coefficient between fitted and observed data.

3 RESULTS

Here, we provide the main results of our periodicity analysis for each object (Figs. 5-10). First of all we show the novel 2D correlation maps of fundamental periodicities for each object, which also depict links between oscillations in the combined light curves. Then we summarize all results in Table 2. Since determined periodicities are not apparent from the observed light curves, Fig. 11 compares them with corresponding sinusoidal fit (Eq. (7)). The estimated parameters of sinusoidal models are given in Table 3.

3C 390.3. The 2D correlation maps in Fig. 5 show the signature of the 6.3 and 7.1 yr period to be present in the continuum and H α line. The method yields ~ 0.7 for the correlation coefficients of both periods with a significance $p < 0.00001$. Somewhat weaker periodicity (correlation coefficient ~ 0.5 , but still significant) was found at 9.5 years. Note, however, that on the same significance level the periods of 4 years and 5.4 years are seen in two light curves but with negative correlation coefficients. Similarly, in the continuum and H β line periods of 10, 8 and 6.4 years are identified with even larger correlation coefficients than in previous case, while periods of 5.4 and 3.6 expressed negative correlation coefficients as in the case of the continuum and H α line. These 'islands' of negative correlation are totally surprising and worthy of further investigation. We found significant periods of 9.4, 6.4, and 3.4 yr (correlation coefficients around 0.8) in the continuum 1370 Å and CIV, while negative correlation, stronger than in the case of H α and H β emission lines, appears at 7.8 and 4.7 yr. On the other hand, largest negative links between oscillations in the continuum 1370 Å and Ly α are seen at 7.1 yr and 10.3 yr, while positive relationship is seen at 6.3 yr. The periods are consistent across all light curves except that correlation coefficients changed polarity differently in the case of IUE light curves. A visual inspection of Fig. 11 shows that multisinusoidal models are quite successful in describing the peaks and troughs of the original data. This is reflected in high correlation between the fitted model and original data (see Table 3). However, χ^2 is large due to inaccurate reconstruction in the large gapped period, because of the lack of data.

Arp 102B. While every period is incidentally correlated with itself (correlation coefficient equals 1 on the diagonal), any transient oscillations having physical origin which are hidden within the light curves should be revealed as clusters close to the diagonal. The main common feature in all correlation maps is the absence of any periodic variability (i. e correlation clusters), even in autocorrelation maps. This is well illustrated in Fig. 6.

NGC 4151. The data set of the H α line is long enough, for our hybrid method to clearly detect periods at significance level $p < 0.00001$. Obtained autocorrelation map (see Fig. 7) revealed three clusters of significant periods (large correlation coefficients) at 5.4, 8.3 and 14 yr in cadence. Phase curves of the continuum and H β line are quite similar to phase curve of the H α line but their main loops are open. Due to this discrepancy in dynamics, detected periodicities of ~ 8 yr and ~ 5 yr (corresponding to the smaller loops in phase curves) in the continuum and H β line are not reported in Table 2. H α is only longer than the continuum and H β due to the two data points (MJD 46511.49 and 47603.29) separated by ~ 3 years. Exclusion of these data points from the H α line produces open phase curve. It appears that these two points

Table 2. Periods in the combined light curves of our sample obtained with the hybrid method. Columns: object name, CLC1 and CLC2 are combined light curves used for periodicity analysis, $P \pm \Delta P$ is determined period and its formal error, r is correlation coefficient corresponding to the period, 95%CI is 95% confidence interval for r , p is significance i.e. p -value for r .

Object name	CLC1	CLC2	$P \pm \Delta P$ [yr]	r	95%CI	p	
3C 390.3	Continuum 5100 Å	H α	9.5 ± 0.3	0.5	(0.49,0.51)	< 0.00001	
			7.2 ± 1.2	0.69	(0.68,0.7)	< 0.00001	
			6.3 ± 0.9	0.68	(0.67,0.69)	< 0.00001	
			4.0 ± 0.04	-0.47	(-0.48,-0.45)	< 0.00001	
			5.44 ± 0.1	-0.35	(-0.37,-0.33)	< 0.00001	
	H β	10.11 ± 0.1	0.77	(0.76,0.78)	< 0.00001		
		7.67 ± 0.02	0.71	(0.7,0.72)	< 0.00001		
		6.42 ± 1.6	0.75	(0.74,0.76)	< 0.00001		
		5.43 ± 0.8	-0.47	(-0.48,-0.45)	< 0.00001		
		3.6 ± 0.4	-0.33	(-0.35,-0.31)	< 0.00001		
	Continuum 1370 Å	Ly α	10.34 ± 0.1	-0.47	(-0.49,-0.45)	< 0.00001	
			7.1 ± 0.02	-0.53	(-0.54,-0.51)	< 0.00001	
			6.25 ± 1.42	0.77	(0.76,0.78)	< 0.00001	
			CIV	9.42 ± 0.02	0.85	(0.84,0.86)	< 0.00001
				7.84 ± 0.02	-0.6	(-0.61,-0.59)	< 0.00001
	6.4 ± 1.22	0.85		(0.84,0.86)	< 0.00001		
H α	4.68 ± 0.7	-0.42	(-0.44,-0.40)	< 0.00001			
	3.4 ± 0.4	0.75	(0.74,0.76)	< 0.00001			
	Arp 102B	Continuum 6200 Å	H α	-	-	-	
Continuum 5100 Å		H β	-	-	-		
NGC 4151	Continuum 5100 Å	H α	13.76 ± 3.73	0.96	(0.956,0.962)	< 0.00001	
			8.33 ± 2.33	0.97	(0.968,0.972)	< 0.00001	
			5.44 ± 1.29	0.98	(0.978,0.981)	< 0.00001	
NGC 5548	Continuum 5100 Å	H β	13.3 ± 2.26	0.87	(0.867,0.873)	< 0.00001	
E1821+643	Continuum 5100 Å	H β	12.76 ± 5.6	0.98	(0.979,0.981)	< 0.00001	
			6.93 ± 1.99	0.80	(0.792,0.808)	< 0.00001	
			4.75 ± 0.79	0.80	(0.792,0.808)	< 0.00001	
	Continuum 4200 Å	H γ	12.36 ± 6.1	0.99	(0.989,0.991)	< 0.00001	
			6.52 ± 3.26	0.91	(0.906,0.914)	< 0.00001	
4.34 ± 0.74	0.94	(0.937,0.943)	< 0.00001				

Table 3. The estimated parameters of sinusoidal best-fitting (Eq. (7)) of normalized observed light curves. Columns: object name, light curve, amplitudes c_i , periods p_i , phases ϕ_i , offsets B , the correlation coefficient between the modeled and observed light curves r , and chi-square goodness of fit χ^2 . Each line represents a set of parameters for one sinusoid.

Object name	LC	c_i	p_i [days]	ϕ_i [radians]	B	r	χ^2
3C 390.3	H β	0.11 ± 0.02	3760 ± 7	6.02 ± 0.01	0.52 ± 0.01	0.81	4.748
		0.05 ± 0.03	2743 ± 15	5.51 ± 0.03			
		0.29 ± 0.04	2300 ± 2	5.47 ± 0.03			
		0.17 ± 0.03	2000 ± 2	0.17 ± 0.005			
		0.08 ± 0.01	1322 ± 1	-5.24 ± 0.1			
NGC 4151	H α	0.22 ± 0.01	5580 ± 435	1.52 ± 4.34	0.63 ± 0.02	0.96	0.381
		-0.07 ± 0.02	2730 ± 422	-4.20 ± 5.63			
		-0.08 ± 0.01	1534 ± 28	-4.02 ± 3.82			
	H α	-0.23 ± 0.01	5165 ± 3	-	0.63 ± 0.01	0.87	1.275
NGC 5548	H β	-0.10 ± 0.01	4378 ± 70	-5.35 ± 1.12	0.40 ± 0.004	0.40	32.804
E1821+643	Continuum 5100 Å	0.16 ± 0.001	4511 ± 1	0.02 ± 0.005	0.71 ± 0.0	0.87	0.449
		0.50 ± 0.0002	2529 ± 0.005	1.57 ± 0.03			
		0.07 ± 0.005	1977 ± 0.1	1.10 ± 0.002			

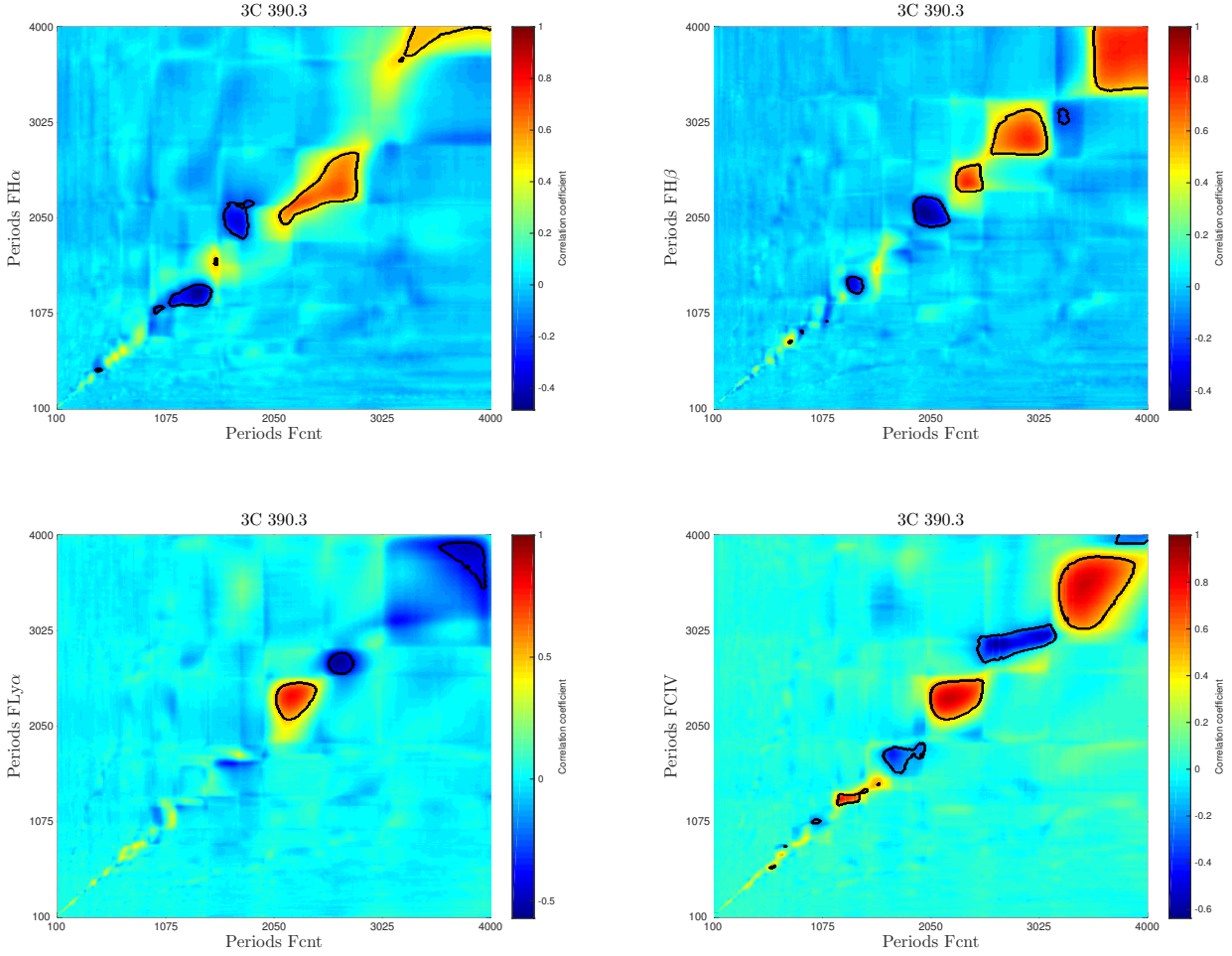


Figure 5. 2D correlation maps of all periodicities within the range 100 – 4000 days found in the light curves of 3C 390.3. In panels the horizontal axes are periods in the continuum at 5100 Å and 1370 Å, respectively. Since correlation coefficients are symmetrical, the upper triangle of each plot is a reflection of the corresponding lower triangle, however, it is presented for better visualization. The areas of high correlation are marked in red. Note the prominent blue clusters of negative correlation. Spurious non-physical signals (such as the dark region at about (1800, 3100) days, in the right bottom panel) appear as uncorrelated (not reflected across the diagonal), because they are uncoupled from real physical processes. Absence of off diagonal correlation clusters indicates that oscillations are caused by physical processes within 3C 390.3.

have quite an effect on the topology of phase curves. The associated multisinusoidal fit is estimate as in the earlier case. The three sinusoid model is undoubtedly superior to one sinusoid model as is evident both, from the correlations between fitted and observed values and from the χ^2 parameter (see Table 3 and Fig. (11)).

NGC 5548. 2D correlation map of the continuum and H β line shows segregation of correlation coefficients into single elongated cluster (see Fig. 8). The cluster is smeared between periods of 11.75 and 14.23 yr. There are no off-diagonal clusters indicating synchronous coupling of period of about 13 yr (approximate center of the cluster) in those light curves. Peterson et al. (2002, see their Table 8) reported significant changes in the H β lag during their 8 yr monitoring program. We tested variability of the time lags between the continuum and H β emission line by means of windowed Z-transformed discrete CCF (Alexander 2013, ZDCF). Both time series were splitted into 20 non-overlapping time segments (of different lengths (T_i)) centered on t_i , $i = 1, \dots, 20$. Each segment encompass either convex or concave parts of the light curve. The results of the ZDCF correlation analysis are summarized in Table 4. In Table 4, the time window used for ZDCF is given in column

win_{ML} . Mean, median sampling and total points in the continuum and H β line segments are given in \bar{P}_{cont} , \hat{P}_{cont} , N1 and \bar{P}_{line} , \hat{P}_{line} , N2, respectively. τ_{ML} is basically the time lag corresponding to the peak of ZDCF τ_{max} nearest to zero lag, and it also has the largest maximum likelihood parameter ML.

In Fig. 9 we show τ_{ML} as a function of the centers of non-overlapping windows presented in Table 4. Even the size of set of time lags may be small, we fit a sinusoid (see Fig. 9), which assumes the periodicity of ~ 4600 days. This function is intended to guide the eye along the data points, not to state that time lags behave necessarily periodic. The fitted curve does not pass through all the points, but we note that about the half of the points are on each side of the curve. It may be worthwhile to mention that there are reasons to expect periodicity in the time lag evolution curve, since BLR size varies with the mean optical luminosity (Lu et al. 2016). By contrast, the estimated sinusoidal fit to the observed light curve (Table 3) is of poor quality, because data are highly volatile, with frequent peaks and troughs, which are often quite sharp (see Fig. 11).

E1821+643. Using the data for all light curves, our method

Table 4. Windowed ZDCF parameters for the continuum and H β emission line segments of NGC 5548. The columns are: win_{MJD} is the time window of the curve in Modified Julian Dates, \bar{P}_{cont} , \tilde{P}_{cont} and N1 stand for the mean, median sampling periods and the total number of points in the continuum segments, respectively. \bar{P}_{line} , \tilde{P}_{line} and N2 are the mean, median sampling periods and total number of points in H β segments. τ_{ML} is time lag corresponding to the peak of ZDCF, possessing the largest maximum likelihood parameter. r_{max} is the peak of ZDCF, and ML is the value of maximum likelihood parameter.

win_{MJD}	Continuum 5100 Å		H β				τ_{ML} (days)	r_{max}	ML
	\bar{P}_{conti}	\tilde{P}_{conti}	N1	\bar{P}_{line}	\tilde{P}_{line}	N2			
41000-42230	26.46	15.80	32.00	17.84	11.89	46.00	25.22 ^{10.66} _{-10.40}	0.96 ^{0.02} _{-0.03}	0.53
41760-42400	22.63	16.10	31.00	16.16	11.89	40.00	25.90 ^{6.58} _{-6.88}	0.98 ^{0.01} _{-0.02}	0.66
42200-42950	24.26	17.40	32.00	22.88	15.97	34.00	21.39 ^{10.54} _{-6.36}	0.83 ^{0.09} _{-0.12}	0.50
42500-43250	22.59	15.70	32.00	23.00	18.95	33.00	7.21 ^{23.39} _{-6.41}	0.53 ^{0.18} _{-0.21}	0.35
43250-44000	10.16	3.60	74.00	15.93	2.06	47.00	7.76 ^{28.01} _{-1.38}	0.68 ^{0.15} _{-0.18}	0.50
44100-44900	11.83	3.90	64.00	29.72	21.90	26.00	22.33 ^{23.26} _{-10.58}	0.69 ^{0.13} _{-0.16}	0.27
44850-45590	10.07	5.00	74.00	30.62	24.93	25.00	20.98 ^{12.61} _{-7.32}	0.70 ^{0.12} _{-0.14}	0.45
45560-47100	9.84	3.90	152.00	36.97	27.08	41.00	23.09 ^{0.02} _{-0.02}	0.29 ^{0.17} _{-0.18}	0.69
47240-48000	5.49	3.00	138.00	4.99	2.00	148.00	12.03 ^{4.36} _{-5.03}	0.84 ^{0.03} _{-0.04}	0.88
47980-48350	8.09	6.00	57.00	4.85	3.00	76.00	8.00 ^{11.78} _{-1.38}	0.94 ^{0.03} _{-0.04}	0.046
48100-48440	10.62	9.00	30.00	5.48	4.00	61.00	8.33 ^{8.88} _{-1.08}	0.91 ^{0.04} _{-0.06}	0.10
48350-48540	8.67	5.00	22.00	4.69	2.00	40.00	9.54 ^{8.58} _{-3.43}	0.64 ^{0.18} _{-0.22}	0.27
48400-48900	3.64	1.00	138.00	5.53	3.00	91.00	16.00 ^{0.49} _{-7.85}	0.94 ^{0.02} _{-0.03}	0.03
48800-49260	1.36	0.39	336.00	4.02	2.00	114.00	10.54 ^{4.79} _{-0.01}	0.79 ^{0.04} _{-0.04}	0.57
49260-49700	3.14	1.00	138.00	3.99	2.00	109.00	16.66 ^{4.59} _{-0.01}	0.57 ^{0.09} _{-0.1}	0.73
49700-50100	4.03	2.00	99.00	4.70	3.00	83.00	16.73 ^{5.07} _{-4.48}	0.93 ^{0.02} _{-0.02}	0.44
50000-50700	1.69	0.57	411.00	3.35	1.00	207.00	22.02 ^{11.99} _{-4.02}	0.78 ^{0.03} _{-0.03}	0.99
50700-51450	2.72	0.90	100.00	4.27	1.00	169.00	22.77 ^{5.50} _{-7.02}	0.87 ^{0.05} _{-0.06}	0.34
51450-52207	3.29	0.99	219.00	8.25	3.00	88.00	17.04 ^{12.95} _{-5.39}	0.55 ^{0.09} _{-0.09}	0.57
52207-56660	31.26	2.00	121.00	56.08	22.00	78.00	28.47 ^{0.01} _{-0.01}	0.69 ^{0.08} _{-0.09}	0.54

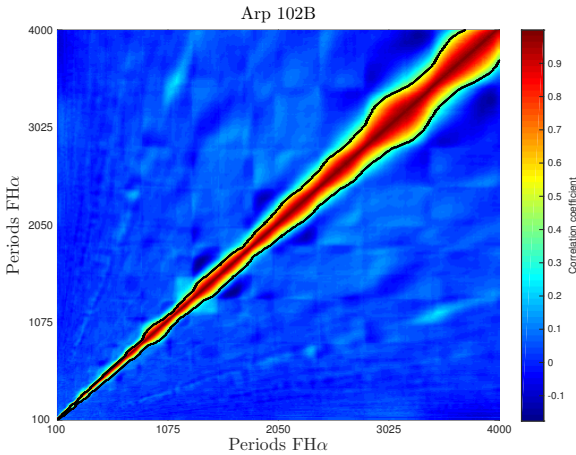


Figure 6. As in Fig. (5) but for the H α of Arp 102B. Note prominent stationarity of diagonal correlation line and absence of correlation clusters.

yielded periods at ~ 12 yr, ~ 6 yr and ~ 5 yr (see Fig. 10). It is interesting that periodicities have been revealed in the case of H β emission line. One can note that the period of ~ 12 yr is about twice of ~ 6 yr period. The correlation maps of E1821+643 show a tail of smaller periodicities disconnected from the prominent cadence of clusters of longer periods, but it is globally similar to the topology of periods found in NGC 4151. Three sinusoids fit is of comparable quality to the case of NGC 4151 (see Table 3).

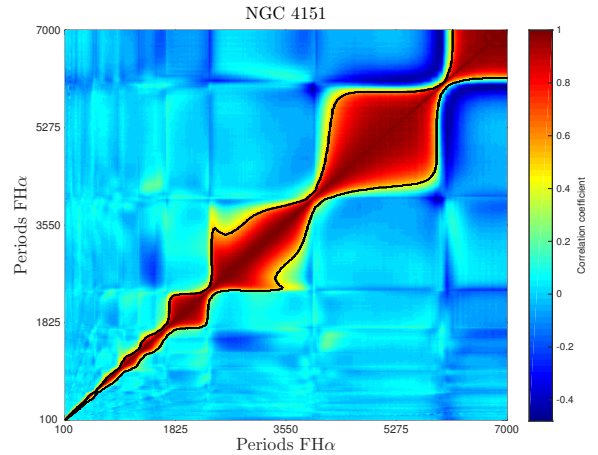


Figure 7. As in Fig. (5) but for the H α of NGC 4151. Note the cadence of correlation coefficients clusters on the diagonal.

4 DISCUSSION

In general, the derived optical periodic variability of our AGN sample is in agreement with previous investigations. However, our hybrid method revealed specific topology of correlation between oscillatory patterns in the light curves that were missed in some other works. Particularly, we can more clearly separate objects according to their oscillatory patterns. In the following, we discuss these oscillatory patterns from the point of view of abstract models of coupled oscillators. For each source we constructed such model which resembles detected oscillatory patterns.

Double-peaked emitters 3C 390.3 and Arp 102B. Our hybrid method made distinction between these two objects based on the

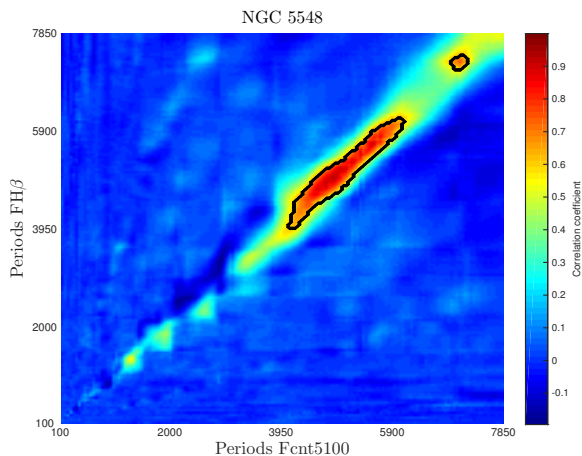


Figure 8. As in Fig. (5) but for the $H\beta$ and the continuum 5100 \AA of NGC 5548. Note a single elongated cluster of correlation coefficients wide about 950 days.

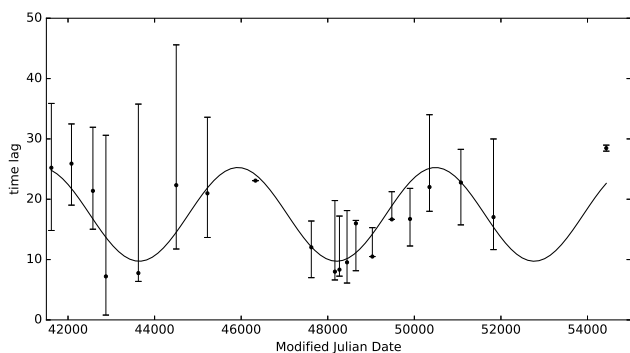


Figure 9. Time evolution of the size of BLR of NGC 5548 compiled from the data given in Table 4. It shows the estimated time lags between the continuum and $H\beta$ emission line from windowed ZDCF against the center of time windows. Superimposed solid line is the best-fitting of a sinusoid of period ~ 4600 days.

presence (absence) of underlying periodic variability, despite that the differences in their shape of spectral lines are subtle. 2D (auto)correlation maps of Arp 102B have simple linear shape, but for 3C 390.3 a manifold of substructures is superimposed. Namely, our analysis has shown the fluctuations in the interactions between the oscillations in the continuum and the emission lines of 3C 390.3 due to substantially different levels of correlation polarity. The clusters of correlations are divided by gaps of very low (or no) correlations, and the islands of correlations switch their polarity (between positive and negative values). This can be seen as an evidence that there exists an activation process which reduces correlation coefficients (from positive values up to zero). After, different relationship is evoked between the periodicities in light curves (e.g. negative correlations). The break off of the correlation band (on diagonal) may be due to the change of variability in the light curves or due to the modulatory effects of some unknown background factors, which may have certain cycles. We applied the hybrid method to a series of artificially non-linear and non-stationary oscillatory signals simulated by Eq. (3) and (4) with unidirectional and bidirectional coupling. The degree of non-linearity/asymmetry is con-

trolled by the ratio (differing from 1) of the periods (frequencies) of the sinusoids. To introduce non-stationary mechanism, we assign a random values between 0 and 10 to the amplitudes of signals, while they were fixed over trial realization, adding the red noise. 2D correlation map of bidirectional coupling of three oscillatory processes (see Fig. 12) is almost matching the map of the real light curves.

We could not produce correlation image with negative 'correlation islands' if the time delays between processes are different. We note that time delays between the continuum and the $H\alpha$ and $H\beta$ lines are ~ 120 and 95 days, respectively, as reported by Shapovalova et al. (2010a). Based on this, one can see the importance of value of time lag for expression of negative link between oscillations which implies that physical places of oscillations sources are somehow functionally related to each other. For example, such relationship can be 'hot spot'. Jovanović et al. (2010) showed that two large amplitude outbursts of the $H\beta$ line observed between 1995 and 1999 in 3C 390.3 could be explained by successive occurrences of two bright spots in the accretion disc. The phase plots in Fig. 13 illustrate comparison between behaviors of the continuum and one of simulated curves from oscillatory network model for 3C 390.3. Both curves show a specific mode of dynamics, generating a major loop (large amplitude oscillation) and the formation of secondary loops (small amplitude oscillations). This confirms that the signal of oscillations is not a monocomponent but a multi-periodic. Both trajectories cover evenly the section of phase space shown here. Particularly, there are no single regulation points at which multiple loops of both trajectories can intersect. The main loops of trajectories are of different diameters due to different amplitudes of real and simulated curves. The secondary loops can be regarded as a hidden attractor.

A specific topology of Arp 102B correlation maps indicates either that periodicities are absent from light curves or that coupling between oscillatory processes is weak. We have created about 100 pairs of artificial curves consisting of 2000 points based on two linearly and weakly coupled oscillators (see Eq. (3)). For reference, the most realistic realization of simulation producing the correlation image matching the linear oscillatory patterns of observed light curves is presented in Fig. 14.

In comparison with 3C 390.3, it seems that with decreased coupling of oscillators of Arp 102B, the clusters merge, decreasing the variance of the distribution of oscillation periods, which eventually results in a system where oscillations are absent. There is a very close match between phase portraits (see Fig. 15) of observed $H\alpha$ and simulated curve demonstrating that the model of weakly coupled oscillators is capable of capturing the dynamics of this object. Note that phase trajectories appear to cross over themselves. Actual trajectories in 3D space (adding the time as third coordinate) are spirals and do not cross. The apparent crossings are due to projection on 2D phase plane. They are similar in topological sense without forming the smaller loops, but they are not closed, indicating either of weak coupling between oscillators or absence of periodicity.

The lack of oscillatory patterns favor non binary BLR hypothesis for this object. This is in line with recent study of Liu et al. (2016), where is reported that the estimated Arp 102B mass of $1.1 \times 10^8 M_{\odot}$ (Shapovalova et al. 2013) is far less than $10^{12} M_{\odot}$ which is obtained under binary black hole assumption. The topology of correlation map of oscillatory patterns of Arp 102B which we found, can be best explained in the context of the process causing gradual variations which are stable over long monitoring period. In spite of both objects 3C 390.3 and Arp 102B being classified as double-peaked emitters, we have shown that underlying

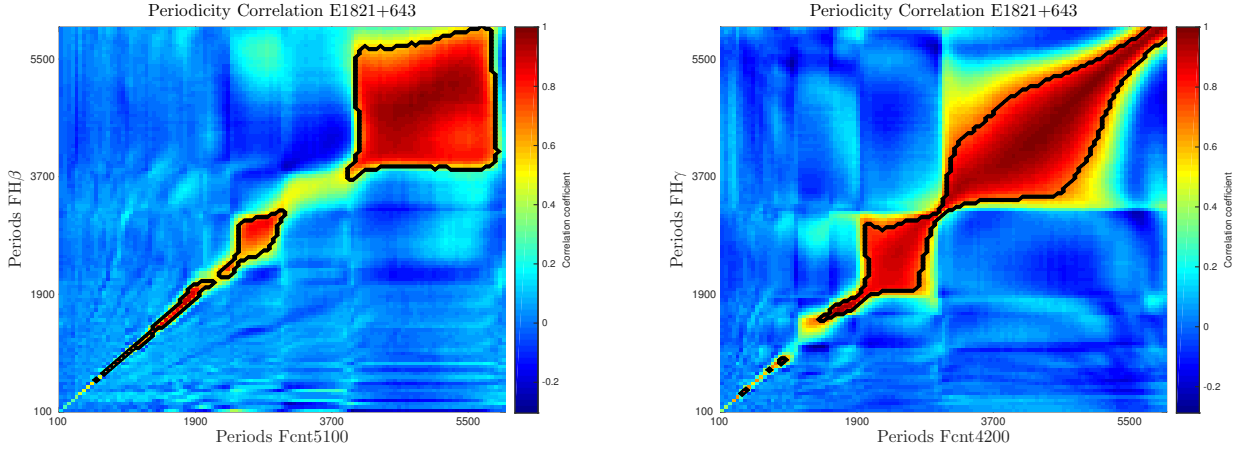


Figure 10. As in Fig. (5) but for all light curves of E1821+643. Left panel: continuum 5100 Å vs. H β emission line. Right panel: continuum 4200 Å and H γ emission line. Note that on both panels the tail of smaller periodicities is disconnected from the prominent correlation clusters.

topology of their oscillations mechanisms are quite different, suggesting different physical background (see detailed discussion in Popović et al. 2011, 2014).

Supermassive binary black hole candidates NGC 4151, NGC 5548 and E1821+643. Again, our hybrid method discerns the oscillatory dynamics of studied objects. Cadenced topology of three detected periods in the H α line of NGC 4151 led us to suspect that periodic signals can be non-linearly coupled. We simulated such coupled oscillatory system using following equation

$$\begin{aligned}
 U_a(t) &= A(t) \cdot \sin(2\pi f_a t + \phi) + cp_{b \rightarrow a} \cdot \\
 &\quad B(t) \cdot \sin(2\pi f_b t + 2\pi f_b \tau) + W(t) \\
 U_b(t) &= B(t) \cdot \sin(2\pi f_b t) + cp_{a \rightarrow b} \cdot \\
 &\quad U_a(t)^2 + W(t)
 \end{aligned} \quad (8)$$

where the non-linear coupling is introduced by squared term $U_a(t)^2$. Simulated curves consists of sum and multiple of base sinus signals of periods of 500 and 300 arbitrary chosen time units. As a consequence, periods of $2 * 500$, $2 * 300$, 500, 300 are accompanied with an interference patterns $500 + 300$, $500 - 300$ (right plot in Fig. 16). Comparing this scenario with autocorrelation of periods in H α (see Fig. 7), the largest period of 13.76 yr can be interpreted as interference pattern (i.e. sum) of two smaller periods of 5.44 and 8.33 yr.

If presented, off diagonal correlations clusters among different periodicities are an indicator of an asynchronous coupling. Note that the correlation map of NGC 4151 does not have such topology, which implies that the coupling between periodicities in this object is synchronous. One way to enhance synchronization among non-linearly coupled oscillators is by increasing the coupling strength between them. Due to this, in the model both coupling strength were set high (see Fig. 16).

The phase portrait of the H α line (see Fig. 17) shows formation of three smaller loops outside of the main loop, confirming multi-periodic oscillations found in 2D correlation map. Moreover, from the same figure it can be seen that the numerical simulation shows similar phase trajectory, except the size and the position of a heart-like smaller loop. This is a consequence of higher amplitude of associated component of oscillations in the model. On both

curves the major loop corresponds to the relatively stable periodic motion of larger amplitude, while smaller loops correspond to the oscillations of smaller amplitudes.

The variability of the continuum and H β line of NGC 5548 over 30 year (Sergeev et al. 2007) and over 40 years (Bon et al. 2016), has revealed sharp peaks which are similar to the case of NGC 4151, suggesting presence of non-linearly coupled oscillations. Moreover, cross correlation functions (CCF) between the continuum and H β line over long time span estimated by (Sergeev et al. 2007, see their Fig. 4) are centered and non deformed, suggesting synchronization between those two light curves.¹ Namely, when the system is asynchronous, the magnitude of the typical CCF values are smaller and asymmetric (i.e. shifted), while synchronous system exhibits larger and centered CCF values. Fig. (18) illustrates the effects of asynchronization between two sine waves with frequencies of $\frac{2\pi}{10}$ on their cross correlation function. The starting phase of one sine wave is 0, while the starting phase of the other sine wave is $-\pi$ and both signals are contaminated with red noise. The calculated CCF is clearly shifted and its values are reduced.

Due to these facts, we considered the same coupled non-linear oscillators model as in the case of NGC 4151, but with three times smaller coupling parameter ($cp_{b \rightarrow a} = 0.2$). Fig. 19 depicts correlation structure of simulated signals. There is pronounced elongated cluster at prevailing period of 500 days. The other period of 300 days is more subtle due to its association with smaller coupling coefficient.

Dominant presence of larger period (i.e lower frequency) is similar to situation described in Farris et al. (2014) where was simulated two-dimensional (2D) hydrodynamical simulations of circumbinary disc accretion in the binary black hole system. They found low frequency mode as dominant component for the case of binary black hole mass ratio $q \gtrsim 0.43$ and that it corresponds to the orbital period of a lump in the inner circumbinary accretion disc, rather than to the orbital binary period. However, their simulation revealed that low frequency is associated with cadence of higher frequency harmonics. Thus, the scenario of the orbiting

¹ That is a consequence of analogy between the CCF and inner vector product. The the inner product measures the angle between two vectors, so CCF can give a sense of the level of the synchronization of two signals.

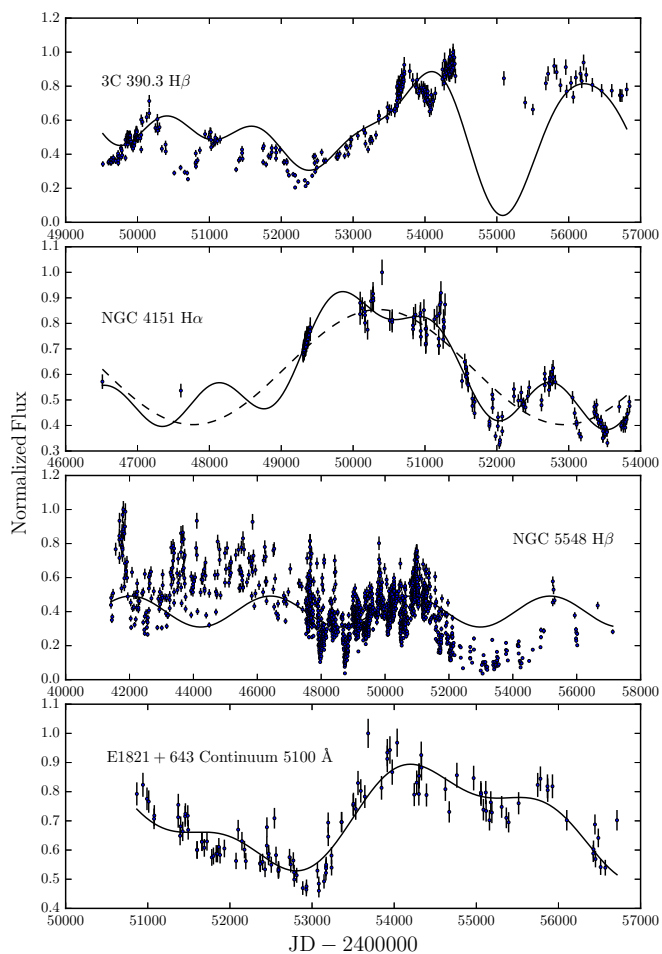


Figure 11. Best-fitting of multisinusoidal models to the observed light curves. Normalized fluxes are represented by dots with error bars whereas models with solid lines. From top to bottom: sum of 5 sinusoids for $H\beta$ line of 3C 390.3; sum of 3 sinusoids (solid line) and one sinusoid corresponding to the largest period (dashed line) for $H\alpha$ line of NGC4151; one sinusoid for $H\beta$ line of NGC 5548 and sum of 3 sinusoids for the continuum 5100 Å of E1821+643. Note that sinusoid model for Arp 102B is missing, since we could not determine any periodicity in its light curves.

lump within the circumbinary disc is more applicable with regard to the cadence of periodicities found in the case of NGC 4151 (see Fig. 7).

The predominant periodic oscillation (~ 12 yr, i.e. ~ 5000 days) can influence other physical properties of this object, i.e. the size of the BLR presumably. From the inspection of Table 4, it is apparent significant variability of the $H\beta$ lags. The time evolution of ZDCF lags shown in Fig. 9 resembles almost periodic behavior of 4600 days, judging by only the data points. However, some of the error bars are very large indicating that within the errors there is no periodicity. We noticed that the largest error bars occurred for the time windows where the dissimilarity between portion of two light curves is evident and/or a few events (flares or dips) are presented in one portion but absent in other. The flares are predominant in the continuum within time windows MJD 42500-43250, 43250-44000, 44100-44900, for which the errorbars are the largest. Possible variations in the $H\beta$ lag have been noticed earlier. Variations of the BLR size of NGC 5548 are between ~ 5 and ~ 30 light days and

they can arise due to numerous physical reasons (see Peterson et al. 1999; Lu et al. 2016).

Moreover, in Fig. 20 has been shown the phase space trajectories of the continuum and simulated curve. In difference to previous cases, distinct periodic waveforms are not present. Namely, instead of regular oscillation, the presence of several limit cycles forming a wide ring is observed which is somewhat similar to the chaotic behavior with random wandering of the states in the phase space. This is in accordance with the large correlation cluster seen in correlation maps of the real (Fig. 8) and simulated curves (Fig. 19). Namely, we can suspect that if the amplitude of driving oscillator is strong enough, period overlapping occurs, which is triggering chaotic behavior. This is in line with the fact that chaos can be born from an overlap of fundamental frequencies of an unperturbed system (Terzić & Kandrup 2004).

For E1821+643, Kovačević et al. (2017) derived averaged periods of 4.78, 5.83 and 12.19 yr from all models of the continuum 5100 Å, 4200Å, and $H\gamma$ emission line. However they could not conclude anything about periodicity in the $H\beta$ emission line due to presented large noise. Its 2D correlation maps are quite similar to the case of NGC 4151. Particularly, if we look at phase portraits of the light curves (Fig. 21) normal limit cycles are observed in the dynamics of E1821+643. They are quite similar to phase portrait of regular sinusoids. We note the presence of two smaller elongated loops in all phase curves reflecting two smaller periods. Also, boundedness of the phase portraits confirms the stability of process. One can think that small variations in the light curves of E1821+643 (e.g. for the $H\beta$ line $F_{var} \sim 7\%$, see Ilić et al. 2017), can be a reason that oscillatory patterns are not distorted. Based on the above discussion, NGC 5548 and E1821+643 represent dynamical extremes, the most chaotic and stable in our sample, respectively.

The correlation of oscillatory patterns in the continuum and emission lines of all objects (except Arp 102B), can be a consequence of a more general correlation trend between the continuum and emission lines fluxes of these objects (see discussion for correlation between continuum and $H\beta$ emission lines of these objects in Ilić et al. 2017). In addition, as time coverage of observations of NGC 4151 continuum is shorter than time coverage of observations of the $H\alpha$ line, our study did not investigate how the weak (or even absent in some time periods) correlation between the continuum and emission line fluxes of this object (see details in Shapovalova et al. 2008) would affect the detection of correlation of their oscillatory patterns. Finally, to investigate the periodic characteristics of the sample, we correlated logarithmic values of obtained periods with AGN optical luminosities and with their BLR sizes. Our findings of absence of any such correlation trend, do not contradict current understanding of relations between those physical parameters of AGN (Lu et al. 2016), but show that it is independent of correlation between continuum and emission line fluxes if presented in the sample. Moreover, the fitting of multiple sinusoids to the observed light curves (see Table 3 and Fig. 11) identified periodicities very similar to those obtained from hybrid method (see Table 2). Thus, all fitted multisine models (except of poor fit of NGC 5548 data) unanimously support the existence of periodicities detected by proposed hybrid method.

It is important to acknowledge that in addition to the signal to noise ratio, errors and irregular sampling, the stochastic behavior in red-noise dominated AGN light curves can easily imitate periods with less than several repetitions, so some of detected periodicities could be due to this effect. It does not imply that the behavior is physically unrealistic, or that it is not occurring in the lines and

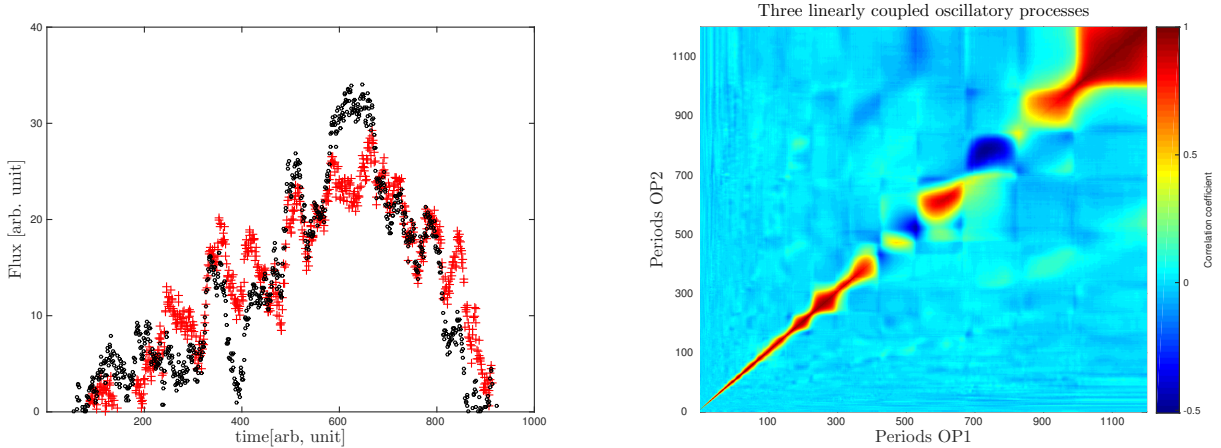


Figure 12. Simulation of bidirectional coupled three oscillators network for the case of 3C 390.3. Left: Random realization of Eq. (4) form two time series (black is $U_a = OP1$, and red is $U_c = OP2$) of amplitudes $A = 1.954$, $B = 1.729$, $C = 2.357$, phase $\phi = \phi_1 = 2.359$ rad coupling strengths $cp_{a \rightarrow b} = 0.7$, $cp_{a \rightarrow c} = 0.5$, $cp_{b \rightarrow a} = 0.2$, $cp_{c \rightarrow a} = 0.3$, frequencies $f_a = \frac{1}{1000}$, $f_b = \frac{1}{300}$, $f_c = \frac{1}{100}$, and time delay of 100 arbitrary chosen time unites. Right: corresponding 2D correlation map, which clearly shows three clusters related to fundamental periods as well as clusters of negative correlation.

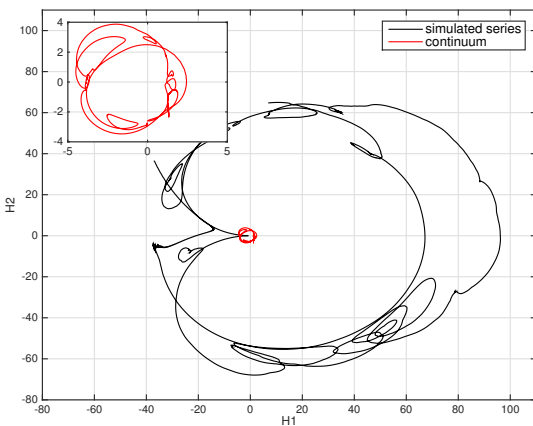


Figure 13. Comparison of the phase trajectories between the continuum of 3C 390.3 and simulated curve OP1 from oscillatory network model in Fig. 12. H1 is related to the time series itself (real part), while H2 is imaginary part of analytical signal (see Eq. (6)). The inset and main plot are very topologically similar (beside a phase shift), showing somewhat distorted ovoid curve.

the continuum in a causal way, just that it is not part of a periodic oscillation.

Whether or not all (or particular) AGN variability could be caused by superposition of many oscillations is an open and controversial question and beyond the scope of our work. However, we note the oscillating structures have been modeled (Tassev & Bertschinger 2004) as particle like (blobs or hot spots, with or without resonant interactions) and waves (oscillating tori, disco-seismic waves). Even derived analytic solutions for accretion discs are stable against finite perturbations, these perturbations could still excite oscillatory behavior. A local restoring forces within accretions discs can rise oscillations (for a details see review Abramowic & Fragile 2013, and references therein) such as: local pressure

gradients running via sound waves, buoyancy forces operating via gravity waves, the Coriolis force acting through inertial waves, and surface waves appearing due to the local effective gravity. Such mechanisms have been argued to power the quasi-periodic oscillations. Particularly, families of oscillations of low order modes are of special interest since they could exist in different accretion disc geometries. Such modes will show tendency to have the largest amplitudes and produce more visible variations than their higher-order complements (Abramowic & Fragile 2013).

5 CONCLUSION

We searched for oscillatory patterns in the new combined light curves of 5 well known type 1AGN using a novel hybrid method and oscillatory network models. The results of our analysis are summarized as follows:

(i) We find strong evidence for periodicities in the combined light curves of 3C 390.3, NGC 4151, NGC 5548 and E1821+643. The absence of oscillatory patterns in the combined light curves of Arp 102B distincts clearly this object from other.

(ii) We constructed the coupled oscillatory models which resemble detected oscillatory behavior in the light curves and confirm their physical background. In the case of Arp 102B the absence of periodicities can be concealed by either unfavorable time series characteristic or sufficiently weak coupling between oscillators mechanisms as our model suggests.

(iii) We demonstrate that dynamics of two binary black hole candidates NGC 5548 and E1821+643 converge to chaotic and stability regime, respectively.

ACKNOWLEDGEMENTS

The authors sincerely thank to the Referee for the constructive comments and recommendations which definitely improve the quality of the paper. L. Č. P. is grateful to the Alexander von Humboldt Foundation for support. This work is supported by

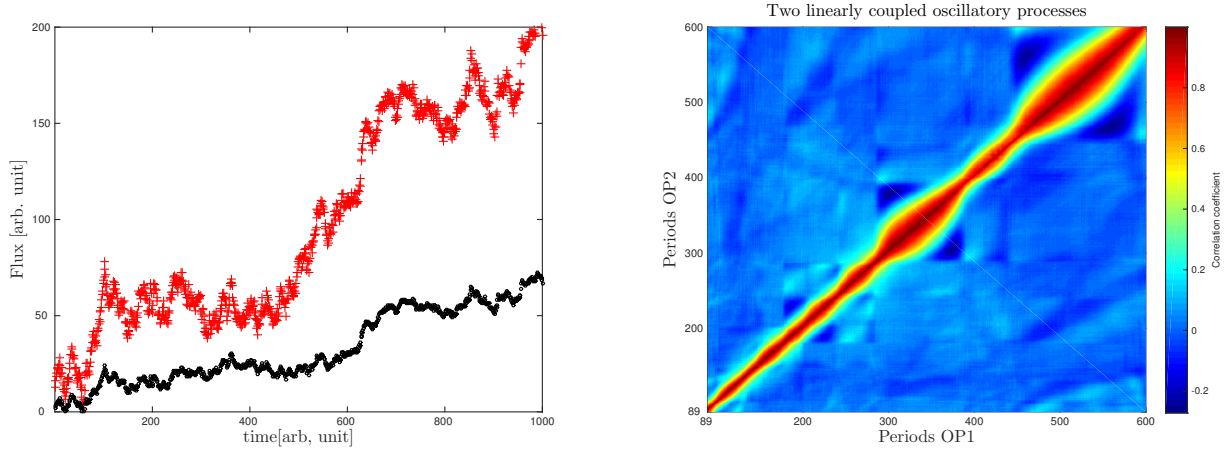


Figure 14. Simulation of two bidirectional coupled oscillators for the case of Arp 102B. Left: Random realization of Eq. (3) form two time series (black is $U_a = OP1$, and red is $U_b = OP2$) of amplitudes $A = 5.29$, $B = 1.99$, phase $\phi = 0.4174$ rad, coupling strengths $cp_{a \rightarrow b} = 0.4$, $cp_{b \rightarrow a} = 0.2$, time delay is 100 and periods are 500 and 300 arbitrarily chosen time units. Right: corresponding 2D correlation map.

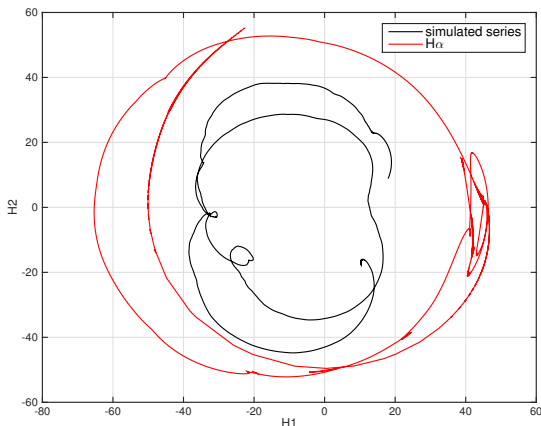


Figure 15. As in Fig. 13 but for the $H\alpha$ line of Arp 102B and simulated OP1 curve from oscillatory model (see Fig. 14). Both curves are similar and non-closed, indicating either weak coupling or absence of periodicity. They appear to intersect themselves due to projection on 2D phase space.

projects (176001) *Astrophysical Spectroscopy of Extragalactic Objects*, (176002) *Influence of collisional processes on astrophysical plasma line shapes* of Ministry of Education, Science and Technological Development of Serbia, INTAS (grant N96- 0328) and RFBR (grants N97-02-17625 N00-02-16272, N03- 02-17123, 06-02-16843, N09-02-01136,12-02-00857a, 12-02- 01237a, N15-02-02101).The work was partly supported by the Erasmus Mundus Master Program, AstroMundus.

REFERENCES

Abramowic M. A., Fragile, P. C., 2013, *Living Rev. Relativ.*, 16, 1
 Afanasiev V. L., Shapovalova A. I., Popović L. Č., Borisov N. V., 2015, *MNRAS*, 448, 3, 2879
 Aghabozorgi S., Shirchorshidi A. S., Wah T. Y., 2015, *Informaton systems*, 53, 16

Alexander T., 2013, arXiv:1302.1508
 Altman D. G, Machin D., Bryant T. N., Gardner M. J., 2000, *Statistics with Confidence - Confidence Intervals and Statistical Guidelines* (2nd edition), British Medical Journal
 Balanov A., Janson N., Postnov D., Sosnovtseva O., 2009, *Synchronization: From simple to complex*, Springer-Verlag Berlin Heidelberg
 Bentz M. C., Katz S., 2015, *PASP*, 127, 947, 67
 Best D. J., Roberts D. E., 1975, *Applied Statistics*, 24, 377
 Bon E., Jovanović P., Marziani P., Shapovalova, A. I., Bon N., Borka Jovanović V. et al. 2012, *ApJ*, 759, 2, id.118
 Bon E., Zucker S., Netzer H., Marziani P., Bon N., Jovanović P., Shapovalova A. I., Komossa S., Gaskell C. M., Popović L. Č., et al., 2016, *ApJSS*, 225, 2, id. 29
 Brøns M., Kaper T. J., Rotstein H. G., 2008, *AIP Chaos*, 18, 015101
 Conover W.J, 1999, *Practical Nonparametric Statistics* (3rd edition), Wiley
 Charisi M., Bartos I., Haiman Z., Price-Whelan A. M., Graham M. J. Bellm E. C, Laher R. R., Márka, S., 2016, *MNRAS*, 463, 2145
 Dietrich M., Peterson B. M., Albrecht P., Altmann M., Barth A. J., Bennie P. J., Bertram R., Bochkarev N. G. et al., 1998, *ApJSS*, 115, 2, 185
 Dietrich M., Peterson B. M., Grier C. J., Bentz M. C., Eastman J., et al., 2012, *ApJ*, 757, 1, id. 53
 Ding H., Trajceviski G., Scheuermann P., Wang X., Keogh E., 2008, *Proceedings of the VLDB Endowment*, Vol. 1, Issue 2, 1542
 Fan J. H., Xie G. Z., Lin R. G., Qin Y. P., Li K. H., Zhang X., 1997, *A&AS*, 125, 525
 Farris B. D., Duffell P., MacFadyen A. I., Haiman Z., 2014, *ApJ*, 783:134
 Grebogi C., Ott E., Yorke J. A., 1987, *Science*, 238, 632.
 Grier C. J., Pancoast A., Barth A. J., Fausnaugh M. M., Brewer B. J., Treu T., Peterson B. M., 2017, *ApJ*, 849, 2, id. 146, 18p
 Grinstead, A., Moore, J. C., Jevrejeva, S., 2004, *Non-linear Processes in Geophysics*, European Geosciences Union (EGU), 11 (5/6), 561
 Guo H., Wang J., Cai Z., Sun M., 2017, *ApJ*, 847,2,1
 Hollander M, Wolfe D.A., 1999, *Nonparametric Statistical Methods* (2nd edition), Wiley
 Hönig S. F., 2014, *ApJL*, 784, 1, L4
 Hawkins M. R. S., 2002, *MNRAS*, 329, 76
 Ilić D., Shapovalova A. I., Popović L. Č., Chavushyan V., Kollatschny W. et al., 2017, *Frontiers in Astronomy and Space Sciences*, 4,12
 Jovanović P., Popović L. Č., Stalevski M., Shapovalova A. I., 2010, *ApJ*, 718,1,168
 Kaspi S., Maoz D., Netzer H., Peterson B. M., Alexander T., Barth A. J. et al., 1996, *ApJ*, 470, 336
 Kawaguchi T., Mineshige S., 1999, *Active Galactic Nuclei and Related Phe-*

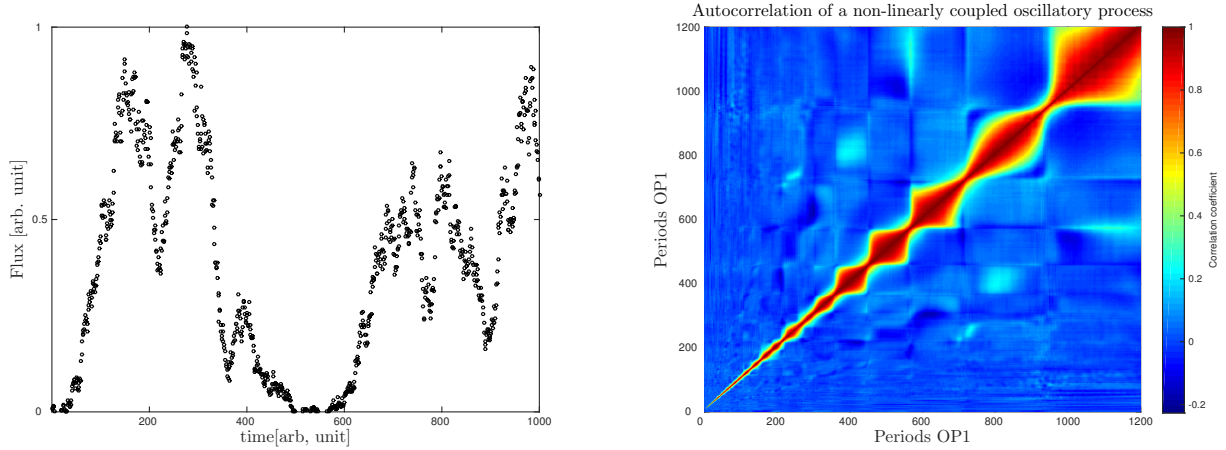


Figure 16. Simulation of two bidirectional coupled oscillators for the case of NGC 4151. Left: Random realization of Eq. (8) form two time series (black is $U_a = OP1$, and red is $U_b = OP2$) of amplitudes $A = 6.09$, $B = 1.04$, phase $\phi = 2.2 \text{ rad}$, coupling strengths $cp_{a \rightarrow b} = 0.7$, $cp_{b \rightarrow a} = 0.6$, periods are 500, 300 and time delay is 100 arbitrarily chosen time units. Note the similarity of sharpness of this signal 'bursts' with features in the observed light curves. Right: corresponding 2D correlation map .

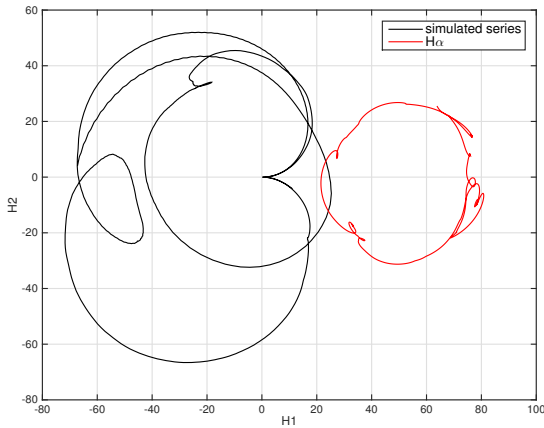


Figure 17. As in Fig. 13 but for the $H\alpha$ line of NGC 4151 and simulated OP1 curve described by Eq. (8) with parameter values as in (see Fig. 16). Note that phase curve of $H\alpha$ line is shifted by + 50 units on x axis for a better view.

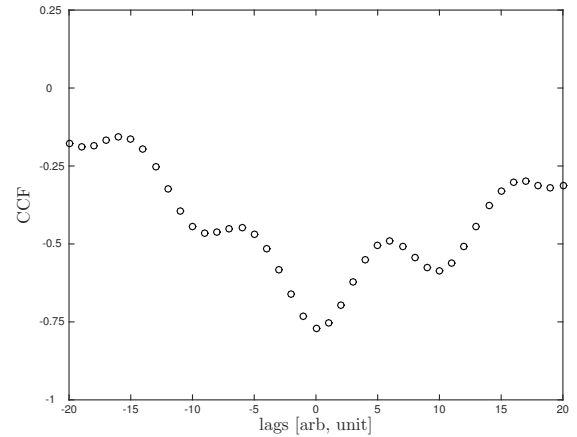


Figure 18. Simulation showing how the cross correlation function is affected by asynchronization between two sine waves. Both signals oscillates with the same frequency of $\frac{2\pi}{10}$ but with different starting phases. Both signals are contaminated with red noise.

nomena, Proceedings of IAU Syposium 194, held 17-21 Aug. 1998, in Yerevan, Armenia. Edited by Y. Terzian, E. Khachikian, and D. Weedman, San Francisco: Astronomical Society of the Pacific, 356

Keogh E., Chakrabarti K., Pazzani M., Mehrotra S., 2001, Knowledge and Information Systems, 3, 3, 263

Kovačević A., Popović L. Č., Shapovalova A. I., Ilić D., 2017, Ap&SS, 362, 2, id.31

Kozłowski S., 2017, A&A, 597, id. A128,1

Kralemann B., Cimponeriu L., Rosenblum M., Pikovsky A., Mrowka R., 2008, Phys. Rev. E 77, 066205

Kralemann B., Pikovsky A., Rosenblum M., 2011, Chaos 21, 025104

Kudryavtseva N. A., Pyatunina T. B., 2006, Astronomy Reports, 50, 1, 1

Kudryavtseva N. A., Britzen S., Witzel, A. Ros E., Karouzos M., 2011, A&A, 526, A51

Lai Y.-C., Ye N., 2003, International Journal of Bifurcation and Chaos, 13, 6, 1383

Lainela M., Takalo L. O., Sillanpää A., Pursimo T., Nilsson K. et al., 1999,

ApJ, 521, 2, 561

Leighly K. M., 2005, Astrophysics and Space Science, 300, 1-3, 137

Li Y.-R., Wang J.-M., Ho L. C., Lu K.-X., Qiu J. et al. 2016, ApJ, 822, 4

Liu J., Eracleous M., Halpern J. P., 2016, ApJ, 817, 1, id. 42

Lu K.-X., Li Y.-R., Bi S.-L., Wang J.-M., 2016, MNRAS, 459, 1, p. L124

Mushotzky, R. F., Edelson R., Baumgartner W., Gandhi P., 2011, ApJL, 743, 12 P

Nakao H., 2015, Contemporary Physics. 57, 1,

Nekorkin V. I., 2015, Introduction to non-linear oscillations, Wiley-VCH, Verlag GmbH & Co. KGaA

Netzer H., 2013, The Physics and Evolution of Active Galactic Nuclei, Cambridge University Press

O'Brien P. T., Dietrich M., Leighly K., Alloin D., Clavel J., Crenshaw D. M., Horne K. et al., 1998, ApJ, 509, 1, 163

Pancoast A., Brewer B., Treu T., 2015a, MNRAS, 445, 3, 3055

Pancoast A., Brewer B., Treu T., Park D. et al., 2015b, MNRAS, 445, 3, 3055

Pering T. D., Tamburello G. McGonigle A. J. S., Hanna E., Aiuppa A.,

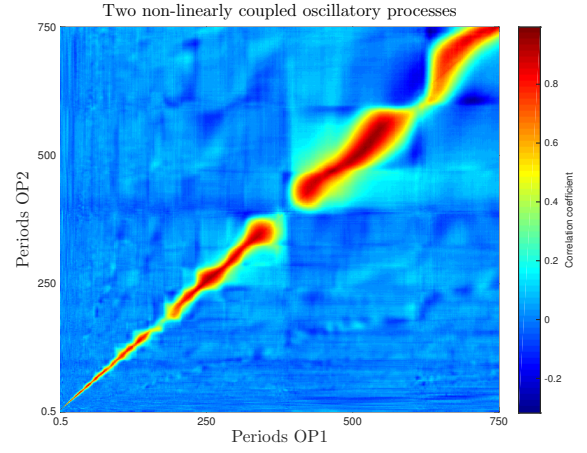
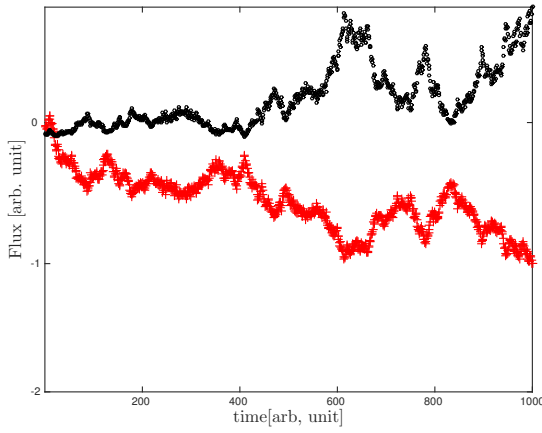


Figure 19. Simulation of two bidirectional coupled oscillators for the case of NGC 5548. Left: Random realization of Eq. (8) form two time series (black is $U_a = OP1$, and red is $U_b = OP2$) of amplitudes $A = 5.92$, $B = 1.27$, phases $\phi = 2.65$ rad, coupling strengths $cp_{a \rightarrow b} = 0.7$, $cp_{b \rightarrow a} = 0.2$, periods 500, 300 and time delay is 100 arbitrarily chosen time units. Right: corresponding 2D correlation map.

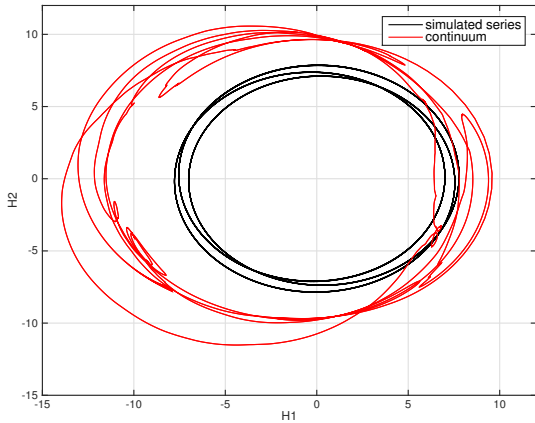


Figure 20. As in Fig. 13 but for the continuum of NGC 5548 and simulated curve (details are given in the text). Note chaotic like appearance of both curves.

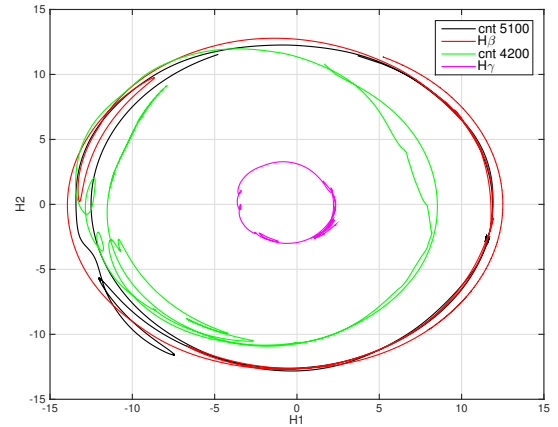


Figure 21. As in Fig. 13 but for the light curves of E1821+643 (details are given in the text). Topology of phase curves is similar to the phase trajectory of regular sinusoids. Note that here the width of rings is drastically reduced in comparison with phase trajectory of NGC 5548 (Fig. 8), so the system is more closer to the simple oscillations.

2014, *Computers & Geosciences*, 70, 206
 Peterson B. M., Barth A. J., Berlind P., Bertram R., Bischoff K., Bochkarev N. G. et al., 1999, *ApJ*, 510, 659
 Peterson B. M., Berlind P., Bertram R., Bischoff K., Bochkarev N. G. et al., 2002, *ApJ*, 581, 197
 Pikovsky A., Rosenblum M., Kurths J., 2001, *Synchronization: A universal concept in non-linear sciences*. Cambridge Non-linear Science Series 12 Eds Chirkov B., Moss, F., Cvitanović P, Swinney H. Cambridge University Press
 Popović L. Č., Shapovalova A. I., Ilić D., Kovačević A., Kollatschny W., Burenkov A. N., et al., 2011, *A&A*, 528, id.A130
 Popović L. Č., 2012, *NewAR*, 56, 2-3, 74
 Popović L. Č., Shapovalova A. I., Ilić D., Burenkov A. N., Kollatschny W., et al., 2014, *A&A*, 572, id. A66
 Rees M. J., 1984, *ARA&A*, 22, 471
 Risaliti, G., Lusso, E., 2017, *Astronomische Nachrichten*, 338, 2-3, 329
 Sergeev S. G., Pronik V. I., Sergeeva E. A., 2000, *A&A*, 356, 41
 Sergeev S. G., Doroshenko V. T., Dzyuba S. A., Peterson B. M., Pogge R. W., Pronik V. I., 2007, *ApJ*, 668, 2, 708

Sergeev S. G., Klimanov S. A., Doroshenko V. T., Efimov Yu. S., Nazarov S. V., Pronik V. I., 2011, *MNRAS*, 410,3,1877
 Sesar B., Ivezić Ž., Lupton R. H., Jurić M., Gunn J. E., Knapp G. R., et al., 2007, *AJ*, 134, 6, 2236
 Simm T., Saglia R., Salvato M., Bender R., Burgett W. S. et al., 2015, *A&A*, 584, A106
 Shapovalova A. I., Doroshenko V. T., Bochkarev N. G., Burenkov A. N., Carrasco L., Chavushyan V. H., Collin S. et al., 2004, *A&A*, 422, 925
 Shapovalova A. I., Popović L. Č., Collin S., Burenkov A. N., Chavushyan V. H., Bochkarev N. G. et al., 2008, *A&A*, 486, 1, 99
 Shapovalova A. I., Popović L. Č., Burenkov A. N., Chavushyan V. H., Ilić D., Kollatschny W., Kovačević A. et al., 2010a, *A&A*, 517, id. A42
 Shapovalova A. I., Popović L. Č., Burenkov A. N., Chavushyan V. H., Ilić D., Kovačević A. et al., 2010b, *A&A*, 509, id. A106
 Shapovalova A. I., Popović L. Č., Burenkov A. N., Chavushyan V. H., Ilić D., Kollatschny W., Kovačević A., Bochkarev N. G. et al., 2013,

- A&A, 559, A10
- Shapovalova A. I., Popović L. Č., Chavushyan V. H., Burenkov A. N., Ilić D., Kollatschny W., Kovačević A. et al., 2016, *ApJSS*, 222, 2, id. 25
- Tassev S. V., Bertschinger E., 2008, *ApJ*, 686, 1, 423
- Tenenbaum J. B., De Silva V., Langford J. C., 2000, *Science*, 290, 2319
- Terzić B., Kandrup H. E., 2004, 347, 3, 957
- Torricelli-Ciamponi G., Foellmi C., Courvoisier T. J.-L., Paltani S., 2000, *A&A*, 358, 57
- Wamsteker W., Wang T.-G., Schartel N., Vio R., 1997, *MNRAS*, 288, 225
- Wang Q., Megalooikonomou V., 2008, *Information Systems*, 33, 1, 115
- Webb J. R., Smith A. G., Leacock R. J., Fitzgibbons G. L., Gombola, P. G., 1988, In: *Supermassive black holes*, Proceedings of the Third George Mason Astrophysics Workshop, edited by M. Kafatos, Cambridge University Press, 66
- Yang W, Tse P. W., 2005, *Journal of Vibration and Acoustics*, 127, 3, 280
- Zheng Z.-Y., Butler N. R., Shen Y., Jiang L., Wang J.-X., Chen X., Cuadra, J., 2016, *ApJ*, 827, 1, id. 56

This paper has been typeset from a $\text{\TeX}/\text{\LaTeX}$ file prepared by the author.